Study of the efficiency of solar panels as a function of incident radiation wavelength

David J. S. Leitão

Instituto Superior Técnico, Universidade de Lisboa, Lisbon, Portugal

***Abstract* — This dissertation investigates the influence of the spectral irradiance variation and the spectral response (SR) on the production of energy by photovoltaic cells. To determine the impact of SR and spectral irradiance on m-Si and Perovskite cells experimental tests were carried outdoors, using optical filters to select different spectrum zones of the solar irradiance. Computational models were developed to simulate different photovoltaic modules, when subjected to a different spectral irradiances, a model with spectral factor (SF). The developed SF model accurately simulated the experiments performed for high-pass filters. The highest relative errors for certain irradiation bands occurred due to the uncertainty of input variables used in the model, which do not fully described the real conditions in the experimental tests. Simulations for the m-Si, a-Si, CdTe and Copper Indium Selenide (CIS) technologies allowed to observe the effect of each SR and of the spectral irradiance for each of them. The CIS technology presented a better overall result in the infrared zone, producing about half of the energy produced by the CdTe technology in the visible zone. The SF, spectral incompatibility factor (MM) and spectral effective responsivity (SEF) parameters were verified to be important for studying the photovoltaic energy production.**

Index Terms* — *Electromagnetic spectrum, Spectral effective responsivity, Spectral factor, Spectral incompatibility factor, Spectral irradiance, Spectral response.

I. INTRODUCTION

The usage of classic sources of energy to satisfy the worldwide energy demand is one of the main causes of the global warming, due to the increase of the amount of polluting gases emitted to the atmosphere [1], causing a high environmental impact, unbalancing ecosystems and affecting human activity in their lifestyle and economy [2]. With this negative impact, global policies have been developed to minimize environmental impacts, which one of most immediate measure is using renewable energy sources [3], [4]. The International Energy Agency (IEA) forecasts that renewable energy will account for two thirds of global investment in power plants by 2040. It is also predicted that solar energy will be the one with the highest growth in electricity production with 74 GW by 2040 [5].

Recent studies have concluded that the variation of the spectral irradiance, Fig. 1, and Spectral Response (SR), Fig. 2, are important aspects in the performance of the photovoltaic devices [6]-[8]. Another conclusion is that the spectral impact depends on the location in terms of latitude, climate, rural or urban environment, among others [6], [9]. Despite the advances made in the study of the influence of irradiance on photovoltaic energy production, models that consider the influence of spectral effects on the field are still limited, contrary to well defined influence of temperature and irradiance in the solar energy electrical production [9].

This paper focuses on the study of the impact of spectral irradiance on a photovoltaic cell, as well as the influence of its SR on its energy production. It is intended to validate a mathematical model that allows the analysis of the impact of spectral irradiance and SR for a photovoltaic cell exposed to a given spectral irradiance. To validate the SF model, experimental tests were carried out and compared with the results obtained by model simulations for the m-Si and organic with Perovskite cells. After the validation of the model, simulations were performed for the m-Si, a-Si CdTe and Copper Indium Selenide (CIS) modules.

One objective of this work is to confirm the possibility of producing photovoltaic energy without visible light, making use of infrared light.

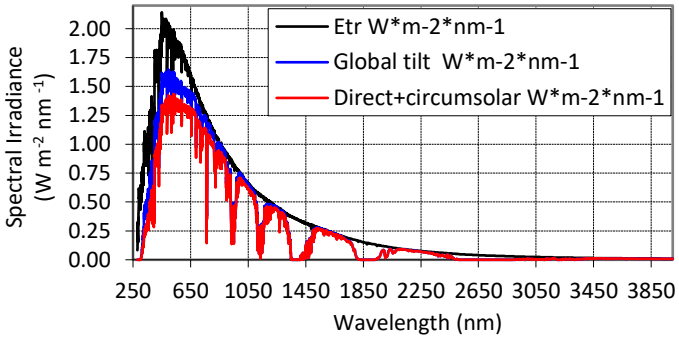

Fig. 1 ASTM G173-03 Sepectral regerence [10], [11].

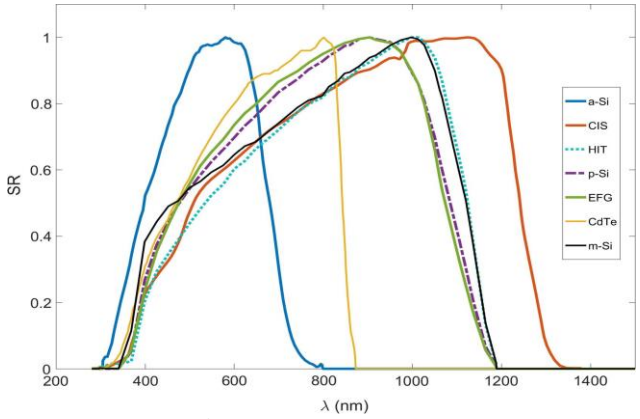

Fig. 2 Spectral Response for various technologies [6].

II. Solar and photovoltaic energy

The solar spectrum consists of different wavelength radiation with different levels of energy, being divided into several regions: γ-rays; *X*-rays; ultraviolet (UV); visible; infrared (IR); microwave; radio-waves; long-waves [12].

A. Solar energy

1) Electromagnetic radiation

The electromagnetic radiation is an oscillation in phase of the electric and magnetic fields, being a propagation of transverse waves, moving in the vacuum at the speed of light, *c*. The electromagnetic waves can be characterized by their frequency, *f*, or wavelength, λ, being related to each other according to eq.(1). From the point of view of quantum mechanics, it is seen as the displacement of photons, which are emitted and absorbed by particles and can be viewed as energy carriers. This energy, *E*, can be calculated by the Planck-Einstein equation (2), where *h* is the Planck constant.

$$\lambda = \frac{c}{f} \tag{1}$$

$$E = h \cdot f \tag{2}$$

2) Sun as a blackbody

The shape of the radiation spectrum emitted by a body has a greater dependence on its temperature. With this, bodies that emit a spectrum of universal character, at a constant temperature are called black bodies. The sun can be considered as a black body at the temperature of 5800 K.

The spectral distribution emitted by a blackbody in a vacuum at a given temperature is given by the Planck equation, (3), where *T* is the body temperature in degrees Kelvin, *k* is the Boltzmann constant and E_λ is the irradiance for a determined wavelength [13].

$$E_\lambda = \frac{2 \cdot \pi \cdot c^2 \cdot h}{\lambda^5} \frac{1}{\left(e^{h \cdot c / \lambda \cdot k \cdot T} - 1\right)} \tag{3}$$

To obtain the total irradiance emitted by the blackbody, G_{bb}, it is required to integrates eq. (3) along all wavelength. In (4), the Stefan-Boltzmann law [14], indicates the power per unit of total area emitted by the surface of an ideal blackbody, where σ is the Stefan-Boltzmann constant.

$$G_{bb} = \sigma \cdot T^4 \tag{4}$$

To determine the solar spectrum outside of atmosphere, the American Society for Testing and Materials (ASTM) has defined a standard spectrum, based on acquired data. This spectrum is called the standard extraterrestrial solar spectrum or Spectral Radiation of Zero Air Mass [11].

B. Solar spectrum and interaction with the atmosphere

The Earth's atmosphere behaves like a protective filter against the action of the harmful extraterrestrial radiation that arrives at our planet and, like a thermal regulator of the Earth, allows conditions necessary to life. The radiation that pass through the atmosphere interacts with the atmospheric components, making the extraterrestrial spectrum different from the terrestrial one. The intensity of these interactions depends on the distance traveled by the radiation in the atmosphere. Under these conditions, ASTM established a standard spectrum with the aim of standardizing a single reference solar spectrum. The currently adopted spectrum indicated in the norm ASTM G173-03 is the one established by ASTM [10]. In Fig. 1 are presented the spectrum AM0, AM1.5 Global and AM1.5 Direct of the ASTM norms.

C. Photovoltaic energy

The photovoltaic effect is the process by which energy from light is converted into electricity in photovoltaic cells. K. Zweibel, [15], explains the photovoltaic effect by saying that light enters a photovoltaic cell and transmits enough energy for some electrons to be released. A power barrier embedded in the cell acts on these electrons to produce a voltage, which can generate a current through a circuit.

The band gap energy is the amount of energy that a photon needs to yield to an electron so that is excited from the valence band to the conduction band. This energy influences the current generated, because the larger the energy required, the smaller is the zone of the spectrum available to form electron pairs. The efficiency of a solar cell is related to the band gap of the semiconductor that constitutes it. The efficiency limit of Shockley Queisser calculated in 1961, is shown in Fig. 3 [16].

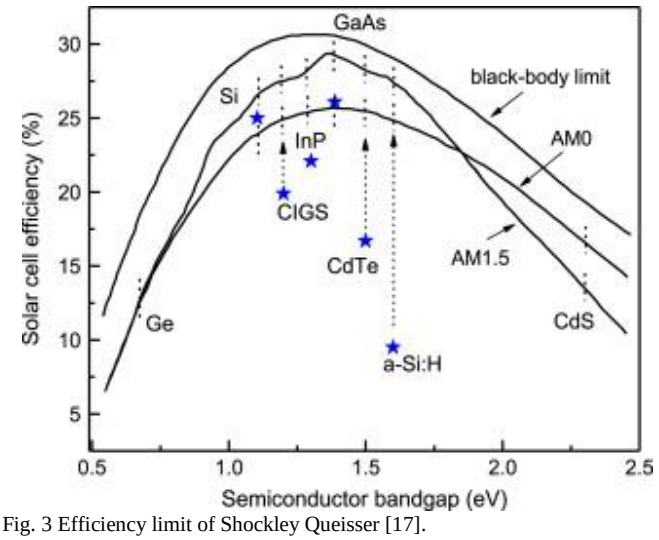

Fig. 3 Efficiency limit of Shockley Queisser [17].

D. Equivalent circuit of a PV cell

PV cells can be modelled by a current source in parallel with a diode, leading to its current-voltage, *I-U*, function given by eq. (5), where I, I_S and I_{ph} are the cell's output current, the dark-saturation current and the photogenerated current, respectively. Parameters U and V_T are the cell's terminal voltage and the thermal voltage, respectively, and n is the diode's ideality factor [18].

$$I = I_{ph} - I_S\left(e^{\frac{U}{n\cdot V_T}} - 1\right) \tag{5}$$

III. Influence of External Parameters

The irradiance influences the value of the short-circuit current, since it is directly proportional to it, eq. (6), where I_{sc} and G are the short-circuit current and the irradiance, respectively, I_{sc}^* and G* are the short-circuit current and the irradiance, both under Standard Test Condition (STC), respectively [18].

$$I_{sc} = I_{sc}^* \frac{G}{G^*} \tag{6}$$

The temperature influences the open circuit voltage, since it decreases with the increasing of the temperature. This occurs because the gap energy is affected by the increase of the temperature, which will affect the saturation current of the diode [18].

A. Spectral Response

The Spectral Response (SR) is the ratio between the photogenerated current of the cell, I_{ph}, and the radiated power falling on it for a given wavelength, indicating how the photons of different wavelengths contribute to the generated current [19]. In this work the SR of four photovoltaics technologies are considered, m-Si, a-Si, CdTe and CIS, which are represented in Fig. 2.

B. Spectral Indexes

1) Spectral Factor

The Spectral Factor (SF) of a non-concentrating PV device is defined as, [6]:

$$SF = \frac{\int E_G(\lambda)\cdot SR(\lambda)\,dy}{\int E_G^*(\lambda)\cdot SR(\lambda)\,dy}\cdot\frac{\int E_G^*(\lambda)\,dy}{\int E_G(\lambda)\,dy} \tag{7}$$

Where the SR(λ) is the SR of the device with the reference temperature as a function of the wavelength, E_G, and E_G^* is the spectral irradiance that effectively reaches the cell and under STC, as a function of the wavelength. From the eq. (7), when SF assumes values higher than one means that the device has a higher energy conversion of the incident spectrum than the reference one in STC conditions. The short-circuit current of a photovoltaic module is proportional to the integration of the product between the spectral irradiance and the SR [6]:

$$I_{sc} \propto \int E_G(\lambda)\cdot SR(\lambda)\,dy \tag{8}$$

Therefore, SF can still be rewritten as, [6]:

$$SF = \frac{I_{sc}\cdot G^*}{I_{sc}^*\cdot G} \tag{9}$$

2) Spectral Effective Responsivity

The Spectral Effective Responsivity (SEF) is defined as, [20]:

$$SEF = \frac{\int E_G(\lambda)\cdot SR(\lambda)\,dy}{\int_{\lambda<\lambda_0} E_G(\lambda)\,dy} \tag{10}$$

Where λ_0 is the upper wavelength at which the absorption takes place in the photovoltaic material. The index expresses in units of A/W, the ratio between the short-circuit current that accounts for irradiance and spectral effects and the spectrum power available for the photovoltaic conversion [19].

3) Spectral Mismatch Factor

The Spectral Mismatch Factor (MM) is defined in the IEC 60904-7 standard [21] as a way of quantifying the relative spectral impact between a sample PV device and a reference PV device by means of:

$$MM_{sample/ref} = \frac{\int E_G(\lambda)\cdot SR_{sample}(\lambda)\,dy}{\int E_G^*(\lambda)\cdot SR_{sample}(\lambda)\,dy}\cdot\frac{\int E_G^*(\lambda)\cdot SR_{ref}(\lambda)\,dy}{\int E_G(\lambda)\cdot SR_{ref}(\lambda)\,dy} \tag{11}$$

Where $SR_{sample}(\lambda)$ represents the spectral response of the sample PV device and $SR_{ref}(\lambda)$ the spectral response of the reference PV device, both at the reference cell temperature. From this definition, $MM_{sample/ref}$ accounts for spectral gains if greater than one or spectral losses if lower than one of the sample PV device with respect to the reference PV device[19].

IV. Methods and Procedures

A. Experimental tests

The experimental tests were carried out to obtain the characteristic curves of m-Si and organic Perovskite solar cells, under the real solar radiation. These tests were done to observe the impact of the spectral irradiance and the SR of the cell in the production of electric energy and also to validate the SF model. For this, several optical filters are used to select the specific zones of the spectrum. With this a structure was constructed to allow to support the cell directly towards the sun and to support the optical filters, Fig. 4.

Fig. 4 Open structure, with m-Si cell.

In addition to the structure, High-Pass (HP), Table 1, [22], and Band-Pass (BP), Table 2, [23]-[24], optic filters, a variable resistance, a voltmeter and an ammeter are used, forming an experimental circuit, as can be seen in the scheme of Fig. 5 and in the experimental set up Fig. 6. The value of the irradiance outside the structure was obtained by using an irradiation meter.

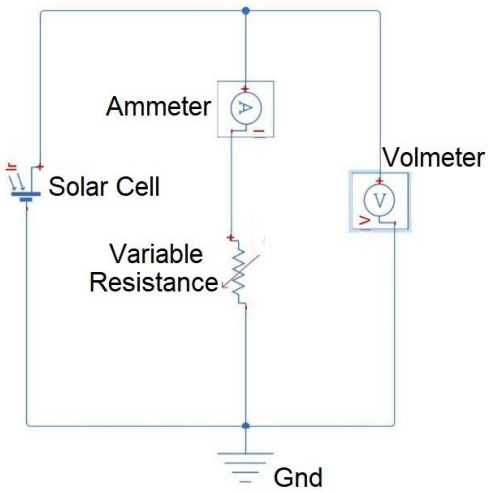

Fig. 5 Scheme of the assemblies of experiments.

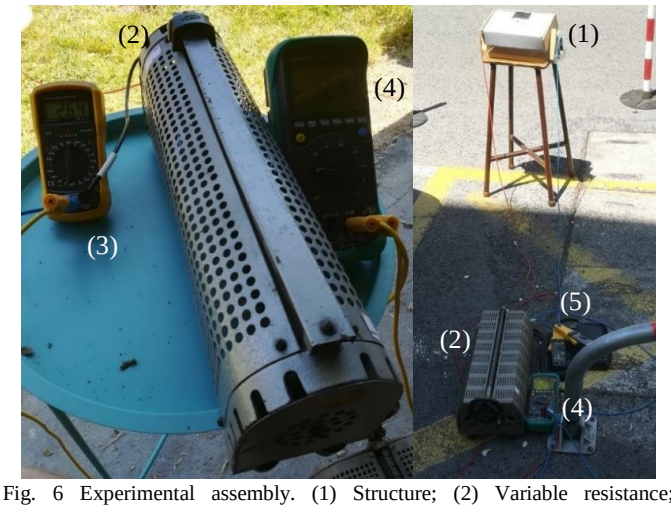

Fig. 6 Experimental assembly. (1) Structure; (2) Variable resistance; (3) Ammeter; (4) Voltmeter; (5) Current probe.

Table 1 High-pass filter characteristics.

Reference	Transmission (%)	Cutting wavelength
FSQ-OG550	90	550 nm
FSQ-OG515	90	515 nm

Table 2 Characteristics of bandpass filters.

Reference	Center wavelength	Bandwidth	Transmission (%)
87-811	1000nm	25nm	99
84-775	700nm	50nm	99
84-774	650nm	50nm	99
84-773	600nm	50nm	99
84-772	550nm	50nm	99
84-771	500nm	50nm	99
84-770	450nm	50nm	99
84-769	400nm	50nm	99

In the addition of the study of m-Si cells, the Perovskite organic cell is used because it is a little studied technology, aiming to analyze the impact of the spectral irradiance in the production of electric energy and to have an idea of its possible SR.

1) Experimental tests with high-pass Filters

The tests without HP filters for the m-Si cell was performed in order to obtain the mean value of the short-circuit current for when the m-Si cell when exposed to the standard spectral irradiance, Fig. 7a). This value is used in the validation of the SF model for HP filters.

The tests for the HP filters were designed to observe the impact on different wide range spectrum bands in the characteristic curves of m-Si and Perovskite organic cells, Fig. 7b).

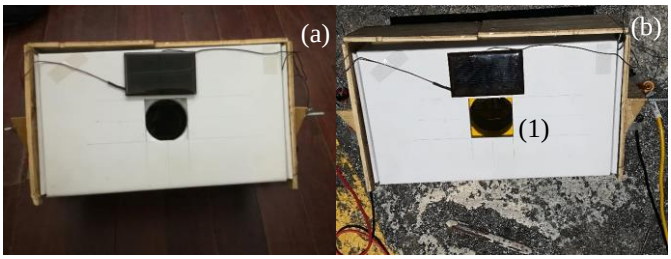

Fig. 7 Structure. (a) No HP filters; (b) With HP filters. (1) HP filter.

2) Experimental tests with band-pass Filters

The tests without the BP filters were performed in order to obtain the mean value of the short-circuit current, when the m-Si cell is exposed to the standard spectral irradiance, since this value is used in validation of the SF model, Fig. 8a).

The BP filters allowed to select a specific zone of the spectrum and to observe the impact of the spectral irradiance and the SR on the photovoltaic energy production in the m-Si and Perovskite organic cells used, Fig. 8b).

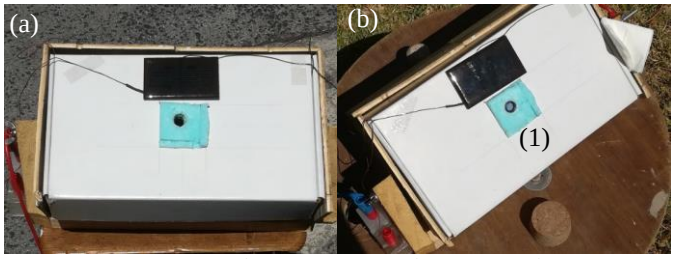

Fig. 8 Structure. (a) No BP filters; (b) With BP filters. (1) BP filter.

B. *Spectral factor model*

The SF model was developed in Matlab with the objective of simulating and studying the performance of several solar cell technologies when exposed to a given local spectral irradiance. For this, it is necessary to validate the model, comparing the experimental results obtained for the m-Si cells with the data generated by the model.

The model makes use of eqs. (7) and (9) to determine SF of the cell and the short-circuit current when it is exposed to a given spectral irradiance.

1) *Simulation for four technologies*

It is intending to use the SF model to simulate different solar modules: Si-m, Si-a, CeTd and CIS, and to analyze how these technologies respond to different zones of the solar spectrum, namely: to the UV, visible and IR. For this, SF, SEF and MM are calculated for each technology, eqs. (7), (10) and (11).

The SR values used for the different technologies are shown in Figure 1 and the module specifications were taken from the datasheets of each module, Table 3, [25]-[28].

Table 3 Specifications of m-Si, a-Si, CdTe and CIS modules.

technology	module	I_{sc} (A)	V_{oc} (V)	module area (m^2)
m-Si	PV-MLU255HC[25]	8.89	37.8	1.656
a-Si	SCHOTT ASI ® 100[26]	3.85	40.9	1.450
CdTe	First Solar Series 6™[27]	2.54	218.5	2.475
CIS	SF170-S[28]	2.2	112	1.228

V. Experimental Results

A. *Experimental tests with high-pass filters*

This section intends to present and compare the experimental data obtained for the experiments performed without the HP filters and the experiments carried out for the HP filters, Table 1, in order to analyze the impact of the variation of the incident spectrum caused by these filters, in obtaining of the characteristic curves of m-Si and organic Perovskite cells.

1) *M-Si cell*

Several tests without HP filters were performed on unfiltered m-Si cells between May 14 and May 21, 2018, between 11:00 a.m. and 4:00 p.m. The HP filter tests were performed between May 21 and June 15 and 19, 2018, between 11:00 a.m. and 4:00 p.m., and a total of six assays were performed for each filter.

As the filters block part of the solar spectrum, the irradiance that reaches the solar cell is limited. This leads to the fact that the experimental results without filters show higher short-circuit current and maximum power values, as expected, however there is no significant variations for the open circuit voltage, Table 4.

Table 4 Values of open circuit voltage, maximum power and respective variations for different tests with and without HP filters for m-Si cell.

	V_{oc} (V)	ΔV_{oc} (%)	P_M (mW)	ΔP_M (%)
No filters	0.563	------	95.35	------
OG 515	0.553	1.78	72.86	23.59
OG 550	0.557	1.07	68.73	27.92

Analyzing Fig. 9, Fig. 10 and the remaining experimental testes, it is observed that the short-circuit current for the OG 515 filter is higher than that of the OG 550 filter, on average 13.33 mA above (corresponding to 7.0% deviation). This is due not only to the radiance difference transmitted by the filters, but also by the spectral response of the m-Si cell.

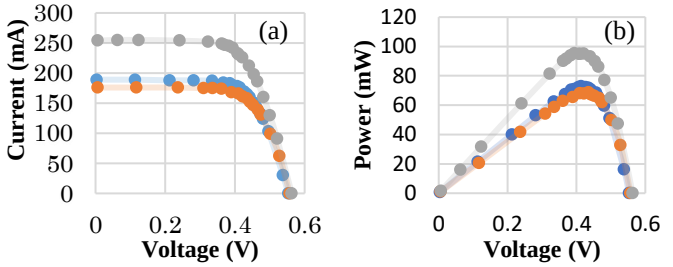

Fig. 9 Experiments performed on 21/05/2018: without filters (-•-), with filter OG 515 (-•-) and filter OG 550 (-•-) for m-Si cell. (a) Voltage-current curves; (b) Voltage-power curves.

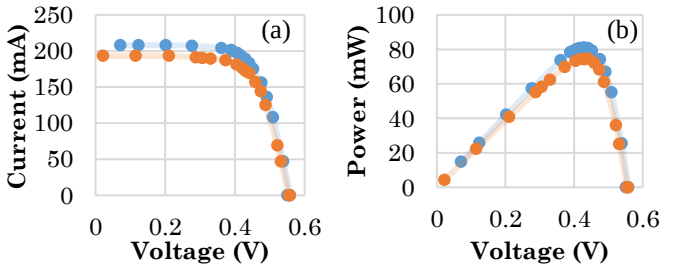

Fig. 10 Experiments performed on 15/06/2018 with filter OG 515 (-•-) and filter OG 550 (-•-) for m-Si cell. (a) Voltage-current curves; (b) Voltage-power curves.

2) *Perovskite organic cell*

Tests were carried out on Perovskite organic cells on May 7, 2018 at 3:45 p.m. and 4:30 p.m., with and without HP filters.

Analyzing the results obtained in the Fig. 11, it is observed that the voltage-current characteristic curves for this technology have an approximately linear shape. The value of the open circuit voltages varies greatly depending on the filter that is used, Table 5, in contrast to the m-Si cell.

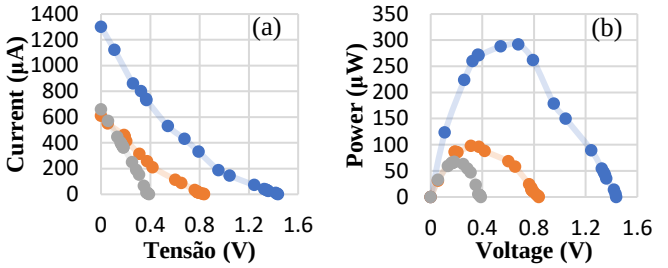

Fig. 11 Tests carried out on 7/08/2018: without filters (-•-), with filter OG 515 (-•-) and those with filter OG 550 (-•-) for Perovskite organic cell. (a) Voltage-current curves; (b) Voltage-power curves.

Table 5 Values of open circuit voltage, maximum power and respective variations for different tests with and without HP filters for Perovskite organic cell.

	V_{oc} (V)	ΔV_{oc} (%)	P_M (µW)	ΔP_M (%)
No filters	0.180	------	292	------
OG 515	0.105	41.7	97.7	66.50
OG 550	0.049	72.9	66.8	77.09

B. *Experimental tests with band-pass filters*

In this section is intended to compare the results of the experimental tests performed with BP filters, Table 2, for m-Si and Perovskite organic cells. As already mentioned these filters have a very narrow bandwidth, allowing passage to very specific zones of the solar spectrum. This leads to the cells receiving low levels of irradiance, which in turn induce lower short-circuit currents than those observed in the tests without the filters.

Based on these experimental results the influence of the SR of each of the technologies and the spectral irradiance in the energy production will be analyzed.

1) *M-Si cell*

From Fig. 12, showing the evolution of the characteristic curves of the cells with the BP filters, together with Table 6, it can be concluded that the response to the 500 nm and 700 nm filters are the ones with a higher maximum power.

However, it is worth remembering that the 1000 nm filter contains a bandwidth of 25 nm, leading to lower power values (0.465 mW). Thus, the maximum power for a 1000 nm filter with a bandwidth of 50 nm is expected to be approximately double that is approximately 0.93 mW, which is the highest value of the BP filters.

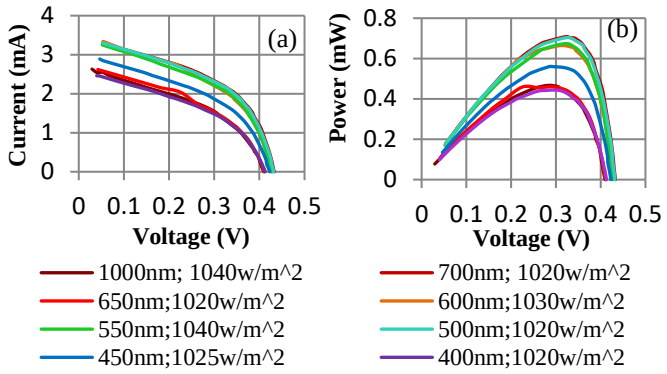

Fig. 12 Tests performed with BP filters on 9/8/2018 for the m-Si cell. (a) Voltage-current curves; (b) Voltage-power curves

2) *Perovskite organic cell*

Similar to the results discussed in section A.2), the results obtained for Perovskite organic cell, Fig. 13, reinforce the hypothesis that the characteristic curve of this technology can be described by a linear equation.

The results shown in Fig. 13 and in

Table 7 show that the 500 nm and 550 nm filters are those with the highest peak power values. Since the 1000 nm filter has half the bandwidth of the rest it is expected that a BP filter of 1000 nm with 50nm bandwidth will have a maximum power of approximately 5.36 µW, exceeding the values reached in the remaining filters.

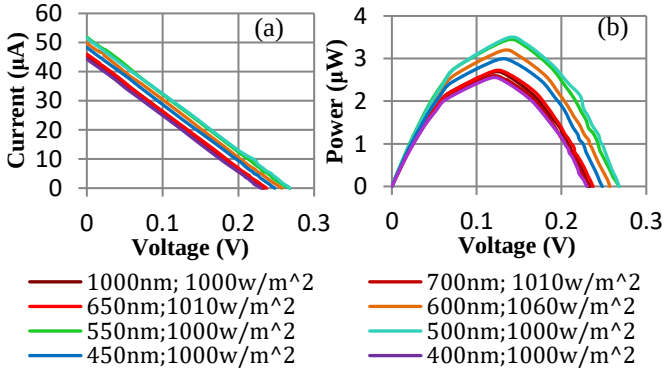

Fig. 13 Tests performed with BP filters on 7/8/2018 for the Perovskita organic cell. (a) Voltage-current curves; (b) Voltage-power curves

Table 6 Values of open circuit voltage, short-circuit current, maximum power and respective variations for the tests with and without BP filters of m-Si cell.

	V_{oc} (V)	ΔV_{oc} (%)	I_{sc} (mA)	ΔI_{sc} (%)	P_M (mW)	P_M (%)
No filters	0.500	----	23.0	----	6.647	100
1000±25nm	----	----	----	----	0.93	14.05
1000 nm	0.410	18.0	2.63	88.51	0.467	7.02
700 nm	0.433	13.4	3.30	85.59	0.708	10.66
650 nm	0.411	17.8	2.62	88.56	0.461	6.93
600 nm	0.426	14.8	3.34	85.42	0.665	10.00
550 nm	0.428	14.4	3.25	85.81	0.674	10.13
500 nm	0.432	13.6	3.30	85.59	0.704	10.59
450 nm	0.423	15.4	2.89	87.38	0.560	8.42
400 nm	0.413	17.4	2.46	89.26	0.444	6.68

Table 7 Values of open circuit voltage, short-circuit current, maximum power and respective variations for the tests with and without BP filters of Perovskite organic cell.

	V_{oc} (V)	ΔV_{oc} (%)	I_{sc} (μA)	ΔI_{sc} (%)	P_M (μW)	P_M (%)
No filters	0.561	----	11.22	----	15.70	100
1000±25nm	----	----	----	----	5.36	34.11
1000 nm	0.234	58.29	45.60	59.358	2.678	17.06
700 nm	0.232	58.68	44.80	60.071	2.586	16.47
650 nm	0.237	57.72	46.00	59.002	2.705	17.23
600 nm	0.257	54.19	49.90	55.526	3.185	20.29
550 nm	0.268	52.23	51.90	53.743	3.429	21.84
500 nm	0.268	52.23	51.60	54.011	3.482	22.18
450 nm	0.248	55.79	48.30	56.952	2.975	18.95
400 nm	0.230	59.00	44.40	60.428	2.540	16.18

Analyzing Fig. 14 which contains the values of the spectral irradiance and the maximum power normalized to their respective maximum values. It is possible to hypothesize that the Perovskite organic cell used in this work will have a better SR in the visible zone up to 550 nm and increase again near 1000 nm. This allows to conclude that this cell has a good use of the irradiance in this zone of the IR. Since no information is available between 750 nm and 950 nm, nothing can be concluded in this range.

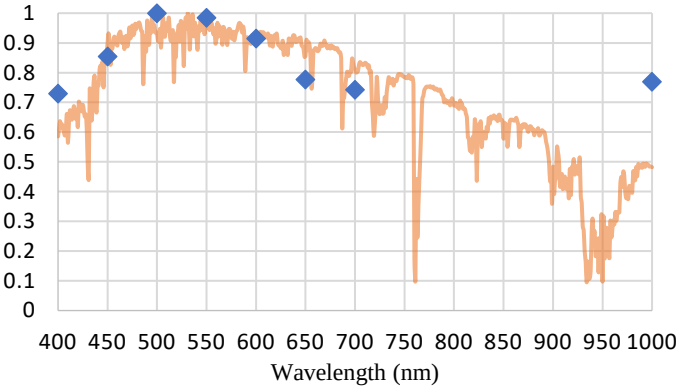

Fig. 14 Normalized Maximum power for BP filters, for Perovskite organic cell, in blue. Spectral irradiance normalized, in orange.

VI. Simulation Results

In this section intend to validate the SF model, comparing the results obtained by simulation with the experimental ones for the m-Si cell and for the different optical filters used. After the validation of the model, it is applied to four different technologies: m-Si, a-Si, CdTe and CIS, to analyze the behavior of these technologies when irradiated with different zones of the solar spectrum.

In Table 8 are the mean values for the short-circuit currents adapted for an irradiance of 1000 W/m^2, for the tests without filters. For a better comparison, the tests without filters were carried out using the supports built for them, since these have different apertures dimensions.

Table 8 Average values of the short-circuit current under STC for the experiments performed with the aperture for filters used.

Experience	I_{cc}^* (A)
Aperture for HP filter	0.271968
Aperture for BP filter	0.030144

A. *Simulation for HP Filters*

This section presents some of the results of the simulations performed to validate the model, comparing these with the experimental results obtained with HP filters for the m-Si cell.

For May 21, 2018, the results for the OG 515 filter with an irradiance of 915 W/m^2, Fig. 15, and for the OG 550 filter with a 910 W/m^2, Fig. 16, are exhibit. In red is the curve that is closest to the experimental data and in yellow the simulated characteristic curve. It is possible to observe that the characteristic curves are close to each other, for the HP filters.

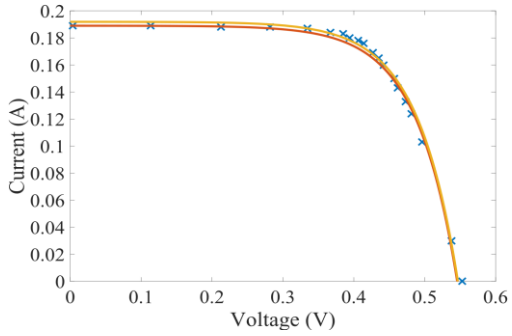

Fig. 15 Experimental data acquired (x), characteristic curve that approaches the experimental data (---), simulated characteristic curve (---); For OG 515 filter.

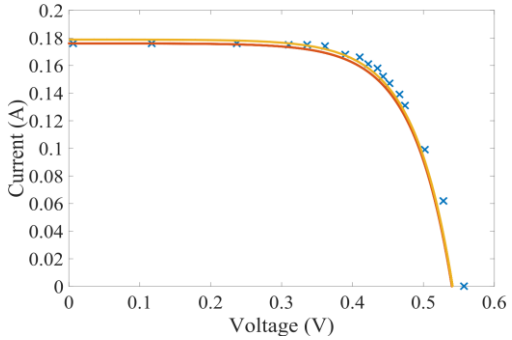

Fig. 16 Experimental data acquired (x), characteristic curve that approaches the experimental data (---), simulated characteristic curve (---); For OG 550 filter.

In Table 9 are presented the values of the short-circuit currents for the experimental and SF model calculated with and without the SF (eq. (6)) for the irradiance incident on the solar cell, as well as the values of the relative errors for both models.

These filters have low relative errors values which propitiate a good approximation of the SF model. However, the variation

of the relative error for the different simulations has the possibility to be related to the variation of the spectral irradiance throughout the days. Another possible explanation is the variation of the SR of the cell with the temperature changing the amount of solar energy converted into electric energy.

B. Simulation for BP Filters

This section presents some of the results of the simulations performed to validate the model, comparing these with the experimental results obtained with HP filters for the m-Si cell.

Simulations were performed for the filters indicated in Table 2. However, in this paper, only is presented simulations for the 650 nm filter, Fig. 17, where the SF model generates a good approximation and for the 400 nm filter, Fig. 18, which obtain the highest relative error values. Although the SF model has high values of relative errors for certain irradiation bands,

Table 10, these errors can be justified by the input variables used by the SF model, which do not fully describe the reality of the experiments performed. As the spectral irradiance variation in these spectrum ranges, the m-Si cell has a SR different from the one used to describe it, or a variation of the bandwidth of the BP filters. For a small variation of these variables causes a considerable variation in the irradiance value that effectively reaches to the solar cell, causing a large variation of the values of the short circuit current within the order of magnitude of this one.

It should be noted that the SF model obtained an average relative error of 33.07%, which may decrease with the use of the appropriate variables, compared to 38.39% obtained for the model without SF.

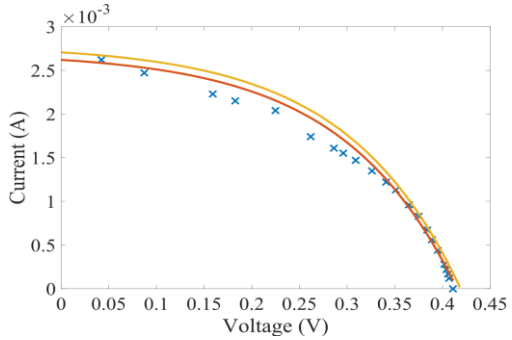

Fig. 17 Experimental data acquired (x), characteristic curve that approaches the experimental data (---), simulated characteristic curve (---); For 650 nm filter.

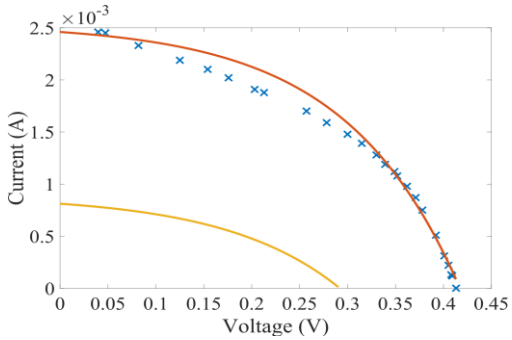

Fig. 18 Experimental data acquired (x), characteristic curve that approaches the experimental data (---), simulated characteristic curve (---); For 400 nm filter.

Table 9 Values of short-circuit current and their respective relative errors for HP filters

Day	Hour	Filter	I_{sc} experimental (A)	I_{sc} SF model (A)	I_{sc} model without SF (A)	Relative error SF model (%)	Relative error model without SF (%)
21/5/2018	15h-15:50h	OG 515	0.189	0.192	0.183	1.53	3.33
		OG 550	0.176	0.179	0.170	1.59	3.35
15/6/2018	12:30h-13:30h	OG 515	0.208	0.203	0.193	2.21	7.45
		OG 550	0.193	0.191	0.181	1.30	6.05
	15:21h-16h	OG 515	0.203	0.209	0.199	3.10	1.83
		OG 550	0.188	0.193	0.185	2.39	1.56
18/6/2018	12:42h-14:16h	OG 515	0.179	0.189	0.180	5.42	0.40
		OG 550	0.166	0.179	0.170	5.30	2.48
19/6/2018	12:23h-12:45h	OG 515	0.180	0.185	0.176	2.56	2.38
		OG 550	0.169	0.179	0.166	3.43	1.56
	13h-13:27h	OG 515	0.182	0.189	0.180	3.68	1.26
		OG 550	0.170	0.179	0.168	5.18	1.04

Table 10 Values of short-circuit current and their respective relative errors for BP filters

	I_{sc} experimental (mA)	I_{sc} SF model (mA)	I_{sc} model without SF (mA)	Relative error SF model (%)	Relative error model without SF (%)
1000 nm	2.63	1.083	0.6	58.82	77.18
700 nm	3.3	2.616	1.953	20.73	40.82
650 nm	2.62	2.706	2.171	3.28	17.14
600 nm	3.34	2.65	2.274	20.66	31.91
550 nm	3.25	2.517	2.328	22.55	28.36
500 nm	3.3	2.231	2.277	32.39	30.99
450 nm	2.89	1.759	2.012	39.13	30.38
400 nm	2.46	0.812	1.221	66.99	50.35

C. *Simulation for BP Filters*

In this section the model developed is used to simulate four solar modules of the m-Si, a-Si, CIS and CdTe technologies, in which SR for each technology is shown in Fig. 2.

The Fig. 19 shows the spectral irradiance converted by the different modules. It is possible to observe the impact of SR of each technology and the spectral irradiance that is effectively converted into electric energy by each technology.

The simulations are carried out considering that the incident spectral irradiance is equal to the reference spectral irradiance, for three different zones of the spectrum, namely UV, Visible and IR, in order to analyze the influence of each of these zones on the production of photovoltaic energy.

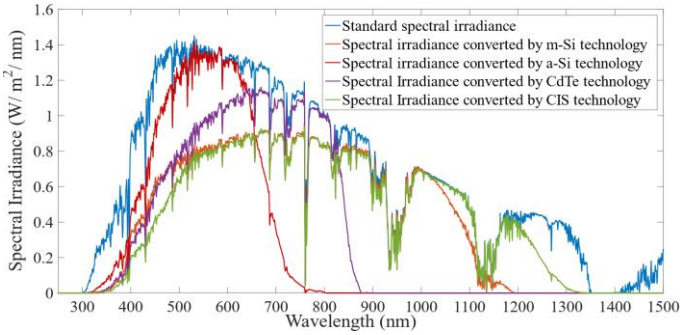

Fig. 19 Spectral irradiance that is effectively converted into electrical energy by m-Si, a-Si, CdTe and CIS technologies.

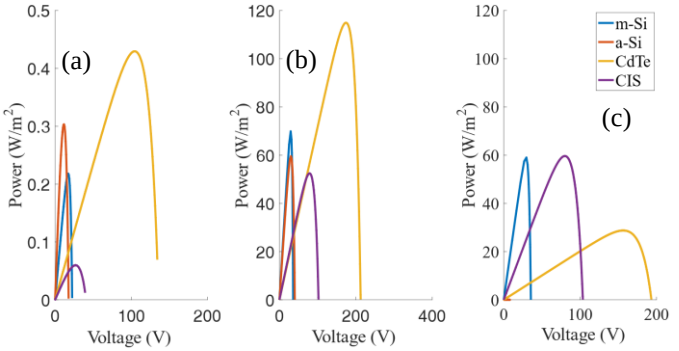

Fig. 20 Simulated voltage-power curves for the m-Si, a-Si, CdTe and CIS modules; (a) UV zone, 250-380 nm; (b) Visible zone, 380-750 nm; (c) IR zone, >750 nm

Observing the Fig. 20, and with the data in the Table 11, it is possible to conclude that in the UV zone the maximum power values obtained are reduced and the a-Si technology has the best SF and a better use of irradiation, however, the CdTe module obtains the higher maximum power values per module area. For the visible zone although the a-Si module obtains the highest SF value, the CdTe module presents the best maximum power values per module area. Finally, for the IV zone the CIS technology presents a better use of the spectral irradiance and performance, generating about half of the power produced by the CdTe technology in the visible zone.

VII. Conclusions and Recommended Works

The main objectives of this work were the study of the impact of spectral irradiance and Spectral Response (SR) on the photovoltaic energy production of the solar technologies used throughout this work.

It has been found that the m-Si cell and Perovskite organic cell respond differently to the various filters used, when exposed to the same spectral irradiance. It was also observed that the Perovskite organic cell has a good SR in the visible zone up to 550 nm, and then also near 1000 nm. Additionally, it has been found that this cell generates voltage-current characteristic curves with an approximately linear shape.

Although the Spector Factor (SF) model has high relative error values for certain irradiation bands, these errors were justified based on the input variables used in the model, which did not fully describe the reality of the simulated experiments performed. It is necessary the more detailed development of this model, considering the possible deviations of the observed conditions.

The simulations performed with the SF model for the m-Si, a-Si, CdTe and CIS modules allowed to observe the effect of SR and the spectral irradiance for each of them, since they have performances and exploitations of the for different areas of the spectrum.

Finally, it was concluded that the SF, the Spectral Mismatch Factor (MM) and the Spectral Effective Responsivity (SEF) are important and necessary factors for the study of photovoltaic energy production. However, they are not enough, and the knowledge of the internal characteristics of the solar modules is also necessary.

It should also be noted that the existing potential in the IV zone, with a significant impact on the production of photovoltaic energy, not only in the experimental tests performed, and also in the simulations performed for the SF model. Thus, the hypothesis of producing electric energy without the presence of visible light was validated.

Table 11 Values of SF, MM, SEF and maximum power per area of each module of m-Si, a-Si, CdTe and CIS for the UV, visible and IR zones.

	SF			*MM*			*SEF*			P_M/A (W/m^2)		
	UV	V	IR	UV	V	IR	UV	V	IR	UV	V	IR
m-Si	0.134	1.098	1.221	1.00	1.00	1.00	0.074	0.607	0.821	0.218	69.855	58.998
a-Si	0.691	2.010	0.007	5.14	1.83	0.01	0.253	0.731	0.014	0.303	59.546	0.018
CdTe	0.226	1.590	0.579	1.68	1.45	0.47	0.100	0.704	0.793	0.429	114.914	28.751
CIS	0.084	0.964	1.396	0.63	0.88	1.14	0.049	0.557	0.824	0.060	52.437	59.638

REFERENCES

[1] PJ Crutzen, "Geology of mankind", *nature International journal of science*, Vol. 415, pp. 23, 2002.

[2] W. Steffen, J. Rockström, K. Richardson, TM. Lenton, C. Folke, D. Liverman, CP Summerhayes, AD Barnosky, SE Cornell, M. Crucifix, JF Donges, I. Fetzer, SJ Lade, M. Scheffer, R. Winkelmann, HJ Schellnhuber, "Trajectories of the Earth System in the Anthropocene" *PNAS*, Vol. 115 (33), pp. 8252-8259, 2018.

[3] P. Chistoff, "The promissory note: COP 21 and the Paris Climate Agreement", *Environmental Politics*, Vol. 25:5, pp. 765-787, 2016.

[4] D. Newbery, MG Pollitt, RA Ritz, W. Strielkowski, "Market desing for a high-renewables European electricity system", *Renewable and Sustainable Energy ReviewsI*, Vol. 91, pp. 695-707, 2018.

[5] International Energt Agency (IEA). Accessed in July 2018 on http://www.iea.org/weo2017/

[6] J. Polo, M. Alonso-Abella, Já Ruiz-Arias e JL Balenzategui, "Worldwide analysis of spectral factors for seven photovoltaic technologies", *Solar Energy*, vol. 142, pp. 194-203, 2017.

[7] D. Dirnberger, B. Müller e C. Reise, "On the uncertainty of energetic impact on the yield of different PV technologies due to varying spectral irradiance", *Solar Energy*, vol. 111, pp. 82-96, 2015.

[8] M. Alonso-Abella, F. Chenlo, G. Nofuentes e M. Torres-Ramírez, "Analysis of spectral effects on the energy yield of different PV (photovoltaic) technologies: The case of four specific sites", *Energy*, vol. 67, pp. 435-443, 2014.

[9] D. Dirnberger, G. Blackburn, B. Müller e C. Reise, "On the impact of solar spectral irradiance on the yield of different PV technologies", *Solar Energy Materials and Solar Cells*, vol. 132, pp. 431-442, 2015.

[10] ASTM G173-03(2012), Standard Tables for Reference Solar Spectral Irradiances: Direct Normal and Hemispherical on 37° Tilted Surface, ASTM International, West Conshohocken, PA, 2012

[11] ASTM E490-00a(2014), Standard Solar Constant and Zero Air Mass Solar Spectral Irradiance Tables, ASTM International, West Conshohocken, PA, 2014.

[12] DL Andrews, "Electromagnetic Radiation", *Encyclopedia of Spectroscopy and Spectrometry (Third Edition)"*, pp. 427-431, 2017.

[13] E. Schubert, "Light Emitting Diodes".

[14] MA Cavalcante e R. Haag, "Corpo negro e determinação experimental da constante de Planck", *Revista Brasileira de Ensino de Física*, vol. 27, pp. 343-348, 2005.

[15] K. Zweibel, "Basic Photovoltaic Principles and Methods", 1982.

[16] W. Shockley e HJ Queisser, "Detailed Balance Limi of Efficiency of p-n Junction Solar Cells", *Journal of Applied Physics*, vol. 32, pp. 510-519, 1961.

[17] V. Avrutin, N. Izyumskaya e H.Morkoç, "Semiconductor solar cells: Recent progress in terrestrial applications", *Superlattices and Microstructures*, vol. 49, pp. 337-364, 2011.

[18] R. Castro, "Uma introdução às Energias Renováveis: Eólica, Fotovoltaica e Mini-hidrica", *IST – Instituto Superior Técnico*, 2011.

[19] PM Rodrigo, EF. Fernándes, FM Almonacid e PJ Pérez-Higueras, "Quantification of the spectral coupling of atmosphere and photovoltaic system performance: Indexes, methods and impact on energy harvesting", *Solar Energy Materials and Solar Cells*, vol. 163, pp. 73-90, 2017.

[20] N. Martín e JM Ruiz, "A new method for spectral characterization of PV modules", *Progress Photovolt.: Res. Appl.*, pp. 299-310, 1999.

[21] IEC 60904-7 (Ed. 3.0), "Photovoltaic Devices - Part 7: Computation of the Spectral Mismatch Correction for Measurements of Photovoltaic Devices", 2008.

[22] Newport, Collored Glass Logpass Filteres. Accessed in April 2018 on https://www.newport.com/f/colored-glass-longpass-filters

[23] Edmund, 1000nm CWL, 12.5mm Dia. Hard Coated OD 4 25nm Bandpass Filter. Accessed in August 2018 on https://www.edmundoptics.com/p/1000nm-cwl-125mm-dia-hard-coated-od-4-25nm-bandpass-filter/30102/

[24] Edmund, Hard Coated OD 4 50 nm Bandpass Filters Accessed in August 2018 on https://www.edmundoptics.com/f/Hard-Coated-OD-4-50nm-Bandpass-Filters/14321/

[25] MITSUBISHI ELECTRIC, modulo PV-MLU255HC. Accessed in March 2018 on https://www.mitsubishielectricsolar.com/images/uploads/documents/specs/MLU_spec_sheet_250W_255W.pdf.

[26] SCHOTT solar, modulo SCHOTT ASI ® 100. Accessed in March 2018 on http://www.solarni-paneli.hr/pdf/shott/SCHOTT%20ASI%20100-107%20data%20sheet%20EN%200111.pdf.

[27] Fist Solar, modulo First Solar Series 6™. Accessed in March 2018 on http://www.firstsolar.com/en-EMEA/-/media/First-Solar/Technical-Documents/Series-6-Datasheets/Series-6-Datasheet.ashx.

[28] SOLAR FRONTIER, modulo SF170-S. Accessed in March 2018 on https://www.desolarstore.nl/wp-content/uploads/2016/09/1400591520wpdm_solar-frontier-sf170-s-eng.pdf.